TOWARDS INDIRECT TISSUE SCAFFOLD FABRICATION VIA ADDITIVE MANUFACTURING AND HYDROXYAPATITE MINERALIZATION

Jesse Bernardo[1], Satyavrata Samavedi[2], Christopher B. Williams[1,3*], Abby W. Morgan[2,4]

[1] Department of Mechanical Engineering, [2] Department of Chemical Engineering, [3] Department of Engineering Education, [4] Department of Materials Science and Engineering
Virginia Polytechnic Institute and State University

ABSTRACT

Unlike traditional stochastic scaffold fabrication techniques, additive manufacturing (AM) can be used to create tissue-specific three-dimensional scaffolds with controlled porosity and pore geometry. Directly fabricating scaffolds through AM methods is limited because of the relatively few biocompatible materials available for processing in AM machines. To alleviate these material limitations, an indirect fabrication method is proposed. Specifically, the authors investigate the use of Fused Deposition Modeling to fabricate scaffold patterns of varied pore size and geometry. The scaffold patterns are then mineralized with a biocompatible ceramic (hydroxyapatite). A heat treatment is then used to pyrolyze the pattern and to sinter the thin ceramic coating. The result is a biocompatible ceramic scaffold composed of hollow tubes, which may promote attachment of endothelial cells and vascularization [1].

In this paper, the authors explore the scaffold pattern fabrication and mineralization processes. Two scaffold pattern materials are tested [acrylonitrile butadiene styrene (ABS) and investment cast wax (ICW)] to determine which material is the most appropriate for scaffold mineralization and sintering. While the ICW could not be thoroughly mineralized despite a sodium hydroxide surface treatment, the ABS patterns were successfully mineralized following an oxygen plasma surface treatment. A 0.004 mm mineral coating was found on the ABS patterns that featured a strut offset of 0.3 mm, which is in the range of appropriate pore size for bone tissue engineering [2].

Keywords: Tissue Scaffold, Additive Manufacturing, Fused Deposition Modeling, Biomimetic Mineralization

1. TISSUE SCAFFOLD FABRICATION

In the event of an injury, the body's extra-cellular matrix (ECM) plays a major role in conducting cells to the injury site and aids in cell spreading, attachment, differentiation, neovascularization and eventual healing of the wound [3-6]. The ECM provides mechanical and structural strength and influences the attachment, movement, differentiation and intracellular signaling so that cells can regenerate and heal injuries. A tissue scaffold is an artificial structure that mimics the ECM and supports three-dimensional tissue formation in order to begin healing an injury [7-9].

The mesostructure of the scaffold (i.e., the size, orientation and geometry of the scaffold's pores) can affect how well cells proliferate throughout the structure [10-12]. An ideal scaffold manufacturing process would allow a designer to control the placement of materials, growth factors and cells throughout the scaffold [13-15]. In addition, the process would also be able to print different types of materials, chemicals, and cells simultaneously. Having the ability to precisely place media and to switch between media types would allow a designer to build tissue-specific scaffolds and maximize effectiveness in regenerating tissue. Unfortunately, existing fabrication techniques do not allow for this level of design freedom.

1.1 Stochastic Scaffold Fabrication

Traditional scaffold fabrication methods include solvent casting and particle leaching [16], gas foaming [17-18], and emulsification, freeze-drying and thermally induced phase separation [19-21]. Briefly, the methods use a liquid scaffold material mixed with a porogen to create a heterogeneous mixture. Once the scaffold is cast in a mold, the porogen is removed through chemical or thermal reactions leaving pores throughout the scaffold. Processing

---

* Corresponding Author: 114F Randolph Hall, Blacksburg, VA, 24061; cbwilliams@vt.edu; (540) 231-3422

conditions often include toxic solvents, high temperatures and long processing times (days to weeks) making it impossible to incorporate cells or growth factors into the scaffold. A specific example is Mikos et al.'s approach to use chloroform and methylene chloride to cast a PLLA scaffold with salts [16]. After evaporating the solvents, salt particles are leached using water. To avoid the use of harsh solvents, Harris et al. compressed a mixture of PLGA powder and salt particles into 3.4 mm thick discs [18]. To saturate the polymer discs, they are pressure treated with 800 psi CO_2 for 48 hours. Following saturation, the pressure is rapidly decreased causing CO_2 to form voids within the disk. The salt particles are then leached – leaving behind a matrix of large (salt) and small pores (gas).

While such processes result in highly porous scaffolds, the size, shape, location and orientation of the porosity is stochastic, and thus is unable to provide repeatable results (Figure 1a). Furthermore, these methods are process dependent and do not allow for the strategic placement of material, and therefore do not allow for control over pore placement and internal architecture.
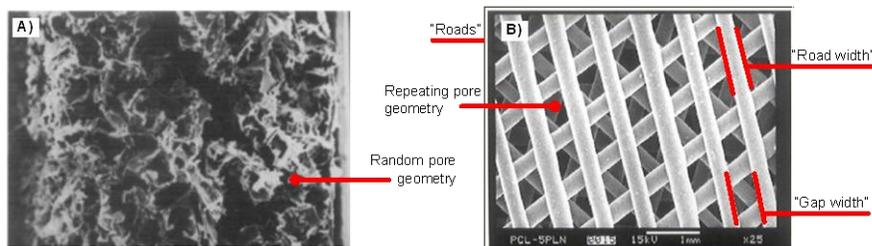
Figure 1. Scaffolds fabricated via **(a)** traditional stochastic (a PLLA "foam" created by a solvent casting particulate-leaching technique [16]) and **(b)** additive manufacturing (a PCL scaffold fabricated via FDM [7]) techniques

1.2 Additive Manufacturing of Scaffolds

Several additive manufacturing (AM) methods have been used to create biocompatible scaffolds with interconnected pores and repeatable geometries including extrusion (FDM, PED, LDM, MDM, PAM, Bioplotting, Robocasting), inkjet printing (D-IJP, I-IJP), and stereolithography (SLA). These layer-by-layer fabrication techniques, in which energy and/or material is selectively patterned to create structural primitives, afford the creation of complex scaffold architectures (Figure 1b). The precision and repeatability of AM affords the creation of scaffold mesostructures that are designed for specific tissues. For example, Oliveira et al. created a bilayered scaffold, that resulted in the differentiation of GBMCs into osteoblasts and chondrocytes in their designed regions [20]. While AM removes most of the design constraints associated with stochastic methods, there still remain several limitations in the scaffold geometries and materials that can be fabricated.

AM processes' reliance on support material to create complex shapes limits the mesostructures that can be fabricated. Since AM builds three-dimensional objects layer-by-layer, the internal voids are often filled with a support material in order to keep overhanging structures from collapsing. The inability to remove entrapped support material is often a limiting factor in determining minimum printable pore size and maximum scaffold thickness. For this reason, extrusion-based processes, such as Fused Deposition Modeling (FDM), are often used for scaffold fabrication since the deposited lines of material ("roads") can span small gaps without the need for support material. The roads are formed by pushing a liquid material through a nozzle where they are deposited onto a substrate. After a layer is completed, the nozzle is repositioned and the new layer is deposited at an offset angle from the previous layer. Using FDM, different pore geometries and sizes can be fabricated by changing the deposited scaffold roads' width (RW), gap width (GW), layer thickness and layer offset angle. Hutmacher and coauthors have used several different road orientation patterns to create different repeating pore geometries [7]. A PCL scaffold with 0-72-144-36-108° road orientation pattern that was fabricated via FDM is presented in Figure 1b.

The primary limitation of fabricating scaffolds via AM is the relatively few biocompatible materials that are compatible with each system. A compilation of the AM processes and materials used in scaffold fabrication are presented in Table 1.

In an effort to address these material limitations, the authors look to an indirect scaffold fabrication process. Sacrificial scaffold patterns are first fabricated via FDM. The scaffold patterns' struts are then coated by a biocompatible ceramic via a surface treatment and a mineralization process. The patterns are then removed via a sintering post-process, resulting in a biocompatible ceramic scaffold composed of hollow tubes.

Table 1. Tissue scaffold fabrication via additive manufacturing: processes, materials and geometries.

	Process Name	Abbr.	Materials	% Porosity	RW	RW/GW	Reference
Extrusion	Fused Deposition Modeling	FDM	PCL; PCL+HA	48-77	0.26-.37	0.16-0.70	[22]
	Precision Extrusion Manufacturing	PEM	Zironia-wax	--	0.1	0.1	[23]
	Low-Temp Deposition Manufacturing & Multi-Nozzle Deposition	LDM & MDM	PLLA-TCP, PDLLA-TCP, PLGA-TCP	89.6	0.5-0.8	0.4	[24-26]
	Pressure Assisted Microsyringe	PAM	PLGA	--	--	--	[27]
	Bioplotting - Hydrogels	--	alginate/fibrin	44-55	~0.35	0.2-0.4	[28]
			polyurethane	52.5	0.66	0.78	[29]
	Robocasting	--	Zirconate, Hydroxyapatite, β-TCP	--	0.1-1.0	0.75-0.60	[30-33]
Inkjet Printing	Direct Inkjet Printing	D-IJP	HA-DTPH, DTPH, PEGDA HA powder	--	-- 0.33	-- 0.45	[34] [35]
	Indirect Inkjet Printing	I-IJP	PLLA, PLGA, Starch, Chitosan	55-99	~0.5/~0.5, some particle leached		[10, 36]
SL	Stereolithography	SL	Poly-4-hydroxybutyrate (P4hB), Polyhydroxyoctanoate (PHOH) PEG	80 --	Pore sizes 0.08-0.18 Channels: 0.15-0.1		[37] [38]

In this paper the authors detail their exploration of the scaffold pattern fabrication and mineralization steps of the overall process. An overview of the proposed indirect fabrication process is provided in Section 2. The experimental setup is described in Section 3. In Section 4, the results of process experimentation are provided. Finally, closure and opportunities for future work are described in Section 5.

2. INDIRECT FABRICATION OF SCAFFOLDS VIA ADDITIVE MANUFACTURING AND MINERALIZATION

2.1 Investment Casting Approches

As a means of circumventing the inherent material processing limitations of existing AM techniques, indirect approaches have been explored. Existing indirect scaffold fabrication techniques typically follow a strategy similar to investment casting. First, a negative mold of the desired scaffold is fabricated, into which a biocompatible slurry is cast. The slurry contains the scaffold material (e.g., HA, PLGA, collagen), solvents (e.g., chloroform and methanol), and porogens [39-41]. The slurry is then solidified via a curing process. After the slurry has set, the mold is removed – leaving behind a biocompatible scaffold.

As an example, hydroxyapatite (HA) scaffolds were created by using SLA [40] and 3DP [42] to create negative molds (Figure 2). In both fabrication processes, a HA slurry was cast in the mold and then dried. The cast was then heated to remove the remaining mold and eventually sintered (around 1300 °C) to increase the density of the HA. Other examples of indirect fabrication of scaffolds are found in Sachlos et al.'s [43] and Yeong et al.'s [41] work with a wax-based direct-IJP process and Lee et al.'s work with a starch-based 3DP process [39].
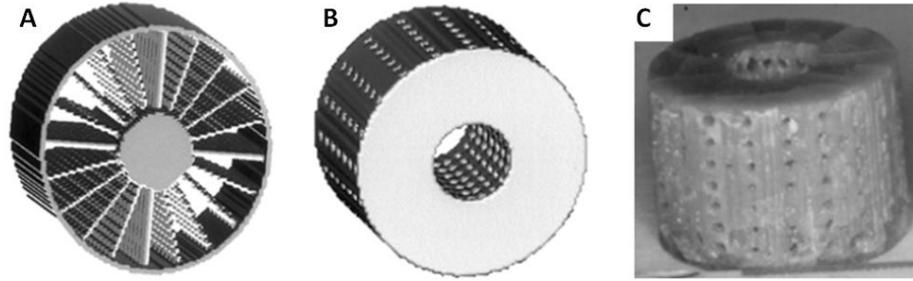
Figure 2. Indirect scaffold fabrication; **a)** a mold "negative" created via SLA; **b)** CAD representation of the desired scaffold architecture; **c)** the final scaffold composed of sintered HA [40]

While such processes provide a means to increase the range of materials that can be processed, the casting process inherently limits the feature sizes that are able to be produced. The viscous casting materials, highly loaded ceramic suspensions, are not able to be introduced into the extremely small geometries typical of scaffolds. Furthermore, casting the materials can trap air bubbles within the mold and cause defects in the scaffold architecture [41]. As a result of the viscosity limitations, the widths of the scaffolds' internal channels and walls fabricated thus far (366 and 800 μm) are larger than other AM produced scaffolds.

2.2 Mineralization of Scaffold Patterns

To overcome the aforementioned limitations with existing indirect scaffold fabrication approaches that are centered in investment-casting, the authors look to ceramic mineralization as a means of creating biocompatible tissue scaffolds with unique, complex geometries. Specifically, the authors propose the following four-step indirect scaffold fabrication process (Figure 3):

1. *Pattern fabrication:* A scaffold pattern with designed pore geometries is fabricated using FDM (Figure 3a)

2. *Surface treatment:* The scaffold pattern is then chemically treated to activate its surface to increase the nucleation sites and to enhance the rate and quality of the mineral deposition.

3. *Mineralization:* The scaffold pattern is then submerged in a simulated body fluid (SBF) solution that deposits layers of biocompatible ceramic (hydroxyapatite, HA) minerals on the surface of the scaffold.

4. *Pattern burnout and mineral sintering:* The mineralized scaffold pattern is then heat treated to pyrolyze the pattern and to sinter the deposited minerals.
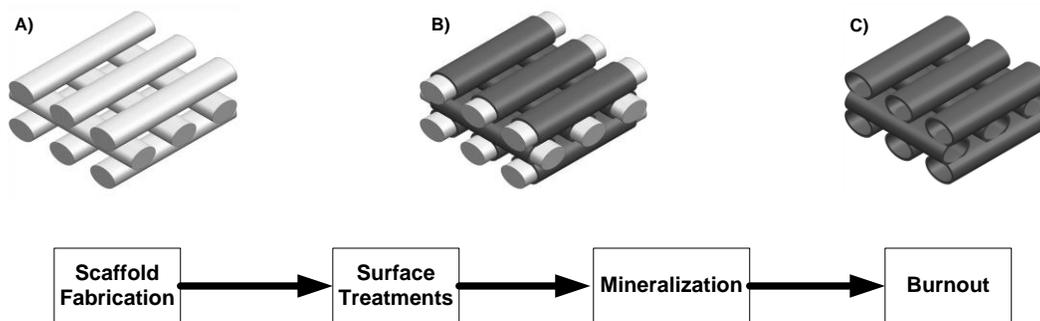
Figure 3. Proposed scaffold fabrication process; a) scaffold pattern is fabricated via FDM, b) scaffold pattern after surface treatment and ceramic mineralization, c) biocompatible scaffold with micro-tubes formed by removing the pattern material.

SBF contains ions which approximate human plasma. The SBF is supersaturated with respect to apatite, with the concentration of HCO_3^- influencing the mineral precipitates [44]. SBF has been used to deposit formations of bonelike apatite, which is essential for material to bond to living bone [45]. Mineralization with simulated body fluid (SBF) has improved the osteoconductive properties of scaffolds [46]. SBF has been used in other research to precipitate apatite particles on a variety of materials including PLLA, PLGA and paraffin microspheres (mineral content was confirmed by XRD and FT IR) [47-48].

The proposed process differs from previous mold-cast techniques as the internal voids of the pattern are not filled with ceramic slurry. Instead, the surface of the pattern is coated with a thin layer of ceramic material (Figure 3b). This simplifies the mold design as there is no longer a need to design a negative mold. Furthermore, by eliminating the use of viscous ceramic slurries, geometry and feature-size limitations found in existing indirect techniques are eliminated.

The resulting scaffold structure is composed of microtubular struts (Figure 3c). These hollow tubes provide additional porosity in the scaffold. This additional porosity may provide sites for scaffold vascularization. As the hollow tubes will decrease the strength of the scaffold, the scaffold will only be suitable for non-load bearing structures, such as in craniofacial scaffold applications.

3. EXPERIMENTAL SETUP

3.1 Pattern Fabrication via Fused Deposition Modeling

FDM is chosen as a means for creating scaffold patterns as it is possible to create complex geometries suitable for scaffold applications without the need for the removal of a secondary support material (Section 1.2). The choice of the pattern material is crucial – the material must be chemically suited for the mineralization process and it must also be suitable for removal via pyrolysis (i.e., must be able to be removed via a heat treatment without significant warping and ash residue). In this work, the authors investigate two materials for the creation of scaffold materials: the standard FDM ABS material (Stratasys, P-400) and an investment-casting wax (ICW) material (Stratasys, ICW-05).

Scaffold patterns are fabricated using a Stratasys FDM 1500 (ABS) and a Stratasys FDM 1600 (ICW) and a T12 nozzle (0.305 mm diameter). The scaffold fabrication printing parameters (i.e., road width (RW), road orientation, temperatures, etc.) used in experimentation are summarized in Table 2. Printed scaffold patterns were 12 mm in diameter, 3 mm in height and printed with a layer thickness of 0.25 mm (5 total layers). Deposited struts were offset by 0.3 mm. This specific gap width (GW) was chosen as bone proliferation has been shown to occur in pore sizes in the range of 0.2 and 0.3 mm [2].

Table 2. Pattern fabrication processing parameters

Material	Processing Temperature (Model/Support/Envelope)	Road Width (mm)	Road Orientation	Printing Pattern
ABS	270 / 265 / 270 °C	0.3	0-90°	Single roads
ICW	70 / 71 / 28 °C	0.4	0-90°	Continuous

To expedite experimentation, the authors developed an in-house algorithm that generates Stratasys Machine Language (SML). The direct creation of SML code circumvented the intermediate steps of FDM (i.e., CAD, STL generation and tool path planning) and allowed for complete control over the fabrication of scaffold geometry and afforded efficient changes to scaffold design and process parameters.

3.2 Scaffold Surface Treatment

Preliminary experiments in mineralizing scaffold patterns without a preliminary surface treatment resulted in incomplete mineralization. Specifically, small groups of minerals crystallized on the surface of untreated ABS scaffolds, but the crystallization was not cohesive (Figure 4a) and failed to coat the bottom surface of the scaffold pattern (Figure 4b).

Thus, the authors looked to the use of a surface treatment to enhance mineralization. Specifically, the authors look to plasma treatment as it has been successfully used in stochastic scaffold processes including PCL [49], and PCL-HA [50]. Plasma treatment activates surface groups for mineralization and decreases the contact angle allowing for aqueous solutions to easily penetrate the scaffold [50]. While a plasma surface treatment was conducted on the ABS scaffolds, the heat of the process is not suitable for the ICW patterns. As such, it was determined to use sodium hydroxide (NaOH) to etch the ICW surfaces.

Plasma treatment for the ABS scaffold patterns was conducted using a SPI Plasma Prep II. The chamber was first cleaned by running for 30 minutes prior to scaffold treatment. The ABS patterns were mounted onto glass slides and inserted into the cleaned plasma chamber. The scaffold patterns were treated in an oxygen plasma for 15 minutes at 50 milliamperes.

| (a) | (b) |
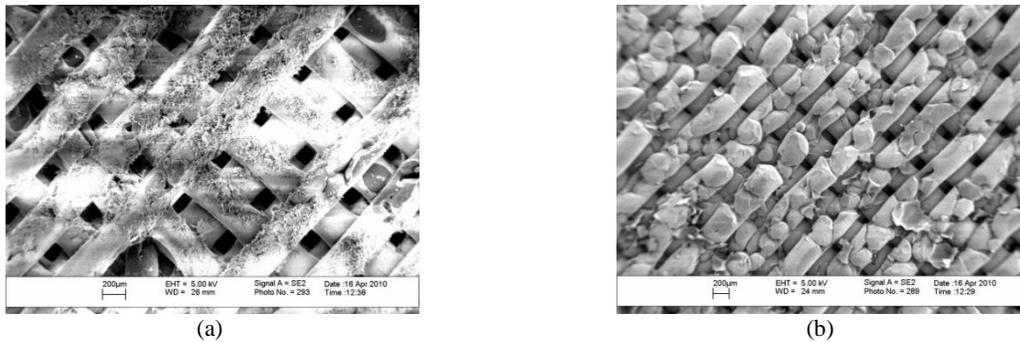
Figure 4. a) FESEM of an untreated ABS scaffold mineralized with SBF 5x (100x zoom); b) FESEM of the bottom of the same scaffold (70x zoom).

Sodium hydroxide creates negatively charged groups on surfaces and is shown to increase mineralization of treated surfaces when compared to identical, non-treated surfaces [46]. For this work, sodium hydroxide was dissolved in deionized water to a molar concentration of 0.1M to treat the scaffold patterns. Scaffold patterns were then immersed in ethanol and placed in a vacuum to remove trapped air bubbles. Deionized water was exchanged with the ethanol, at which point the pattern was immersed in 0.1 M NaOH for 15 minutes. After treating the surface, the patterns were rinsed three times in deionized water to remove any remaining NaOH and then transferred to a Petri-dish for mineralization.

3.3 Scaffold Mineralization

Mineralization of both scaffold types occurred in a simulated body fluid solution (SBF). A concentrated SBF formulation (5x) was used because it accelerates formation of minerals and is stable for long periods of time [44, 48]. To prevent premature precipitation two aqueous solutions were prepared. A "stock" solution contained all of the ions (Table 3) except for the bicarbonate, while the other aqueous solution contained only the bicarbonate. The two solutions could be stored for an extended period of time because precipitation would not occur until the two solutions were mixed. This afforded the creation of large volumes of "stock" and "bicarbonate" solutions that could be quickly mixed together to form SBF 5x when needed.

Table 3. Ion concentrations (mM) of human blood plasma, 1xSBF, 5xSBF

Ion	Blood Plasma	1xSBF	5xSBF
NA^+	142	145.2	710
K^+	5.0	5.0	25.0
Cl^-	103	152	760
Ca^{2+}	2.5	2.5	12.5
Mg^{2+}	1.05	1.5	7.5
$H_2PO_4^-$	1.0	1.0	5.0
SO_4^{2-}	0.5	0.5	2.5
HCO_3^-	27.0	4.2	5.0
pH	7.2-7.4	7.4	6.2

Stock solution is prepared by adding salts (in order that they appear in Table 4) to a flask of 1.0 L of deionized water. Each salt was added and allowed to completely dissolve before the next salt was added. After all salts were completely dissolved, an additional 600 ml of deionized water was added to the stock solution. The bicarbonate solution was prepared by dissolving 0.84 g of sodium bicarbonate in 400 ml of deionized water. The separate solutions were stored in a refrigerator for later use. Stock and bicarbonate solutions are allowed to reach room temperature and then combined in a volume ratio of 4:1, respectfully, to form 5xSBF when needed.

Scaffold patterns were anchored to the center of a Petri-dish containing 50 ml of mixed SBF. The samples were then covered and placed on an orbital shaker inside an incubation chamber set at 37 °C. The samples were removed from the incubator every six hours so that the SBF could be exchanged with fresh SBF. Replacing SBF ensured that the ion concentration remained at a level that produced HA mineralization. The SBF pH (6.2) was monitored throughout the 36 hour cycle.

Table 4. Required salt masses to prepare stock and bicarbonate solutions.

	Salts	Grams
Stock Solution	$NaCl$	81.23
	KCl	3.73
	$CaCl_2 \cdot 2H_2O$	3.68
	$MgCl_2 \cdot 6H_2O$	3.05
	NaH_2PO_4	1.20
	Na_2SO_4	0.71
Bicarbonate Solution	$NaHCO_3$	0.84

After mineralization, the scaffolds were removed and allowed to dry in a desiccant box overnight. Samples were prepared for field-emission scanning electron microscope (FE-SEM) and imaged by the Nanoscale Characterization and Fabrication Laboratory at Virginia Tech.

4. RESULTS

4.1 Pattern Fabrication

Initial efforts in printing scaffolds directly onto the build platform resulted in the fusing of the bottom layer of the scaffold (Figure 5a). As such, a preliminary base layer of sacrificial support material was deposited to provide an even base onto which the scaffold pattern material could be deposited (Figure 5b). Stratasys P-400 release material was used as a base layer for the ABS patterns, while Stratasys-ICW 05 release material was used as a base layer for the ICW patterns. This base layer removed easily from the scaffold patterns (Figure 5c) and prevented fusion of the initial scaffold layer (Figure 5d).
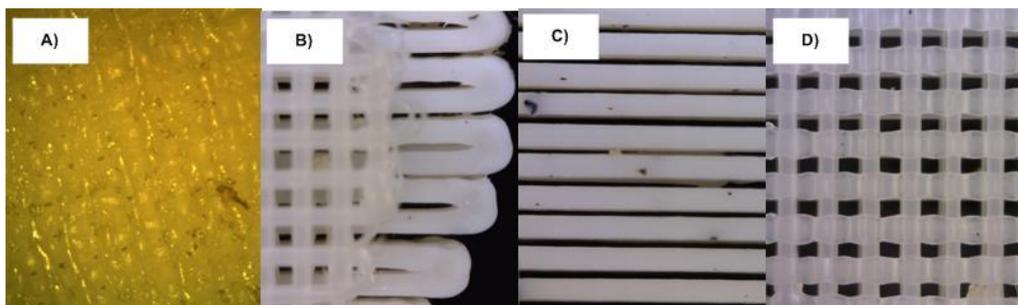
Figure 5. A) Scaffolds not printed on a base had fused bottoms and sometimes failed during printing. B) Scaffold pattern printed on a support material base. C) The scaffold pattern removed easily from the base. D) Scaffolds printed on a base did not have a fused base and had consistent pore sizes throughout.

The pattern fabrication process was well controlled and resulted in consistent RWs for both ABS and ICW. Consistent RWs made it easier to calibrate the machine to print the desired RWs of 0.3 mm (Figure 6). Due to their direct control over the extrusion head via the SML code, the authors were able to develop motions that enabled the deposition of individual scaffold ABS fibers, instead of the serpentine deposition patterns typically found in extrusion-based scaffold fabrication (Table 2). The ability to print individual roads increases the overall porosity of the scaffold, as serpentine deposition patterns close the ends of each deposited layer. It should be noted however, that the ICW patterns were deposited via a traditional serpentine tool path, as it was not possible to print individual roads with that material.

Figure 6. (a) Printed ICW (red) and ABS (white) scaffolds patterns with (b) a gap width of 0.30 mm.

4.2 Surface Treatment and Mineralization

Sodium Hydroxide Etch of ICW Pattern

Sodium hydroxide etch of the ICW pattern showed improved mineralization when compared to mineralization without surface treatment. However, the mineralization was not complete (Figure 7a). As can be seen in Figure 7, only small amounts of mineral can be seen on the ICW as compared to the plasma-etched ABS. As such, further experimentation with ICW was discontinued as it could not be successfully mineralized.

(a)   (b)
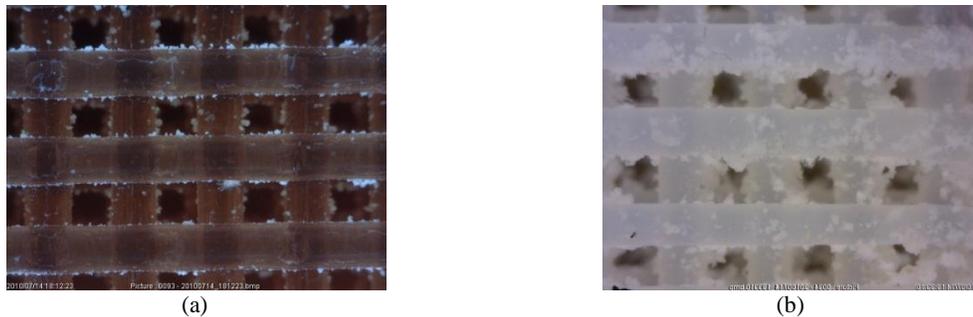
Figure 7. a) ICW pattern has slight mineral deposits following NaOH etch, but is not heavily coated (b) like the ABS pattern following plasma-etch.

Plasma Treatment of ABS Pattern

Following the surface treatment and mineralization post-process, it was observed (via FE-SEM) that mineral deposition had penetrated and uniformly coated the plasma-etched ABS scaffold patterns. Evidence of this coating can be seen in Figure 8a – the darker areas represent the center of the deposited ABS road that is exposed due to the removal of the tape that anchored the scaffolds, while the lighter areas show the deposited mineral coating.

Figure 8b shows that some cracks have formed throughout the mineral coating. This cracking is possibly due to the rapid cool-down that followed mineralization; these cracks can be ameliorated via an annealing process. As seen in Figure 9a, the coating was predominately uniform throughout the scaffold, although small conglomerates did appear. Images of the fractured mineral coating (that resulted from the removal of the tape) showed that mineralization resulted in a coating that is ~0.003-0.004 mm thick (Figure 9b). It is hypothesized that the deposited mineral coating can be thickened by extending the mineralization time.

(a)   (b)
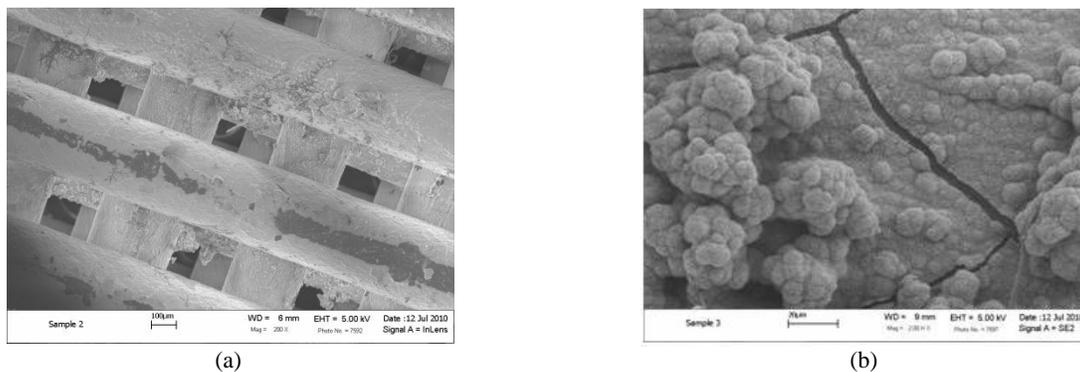
Figure 8. a) Mineralization of the top and second layer of an ABS scaffold (200x zoom). b) Clusters of minerals and small cracks formed on the mineral coating (2000x zoom

928

(a)	(b)
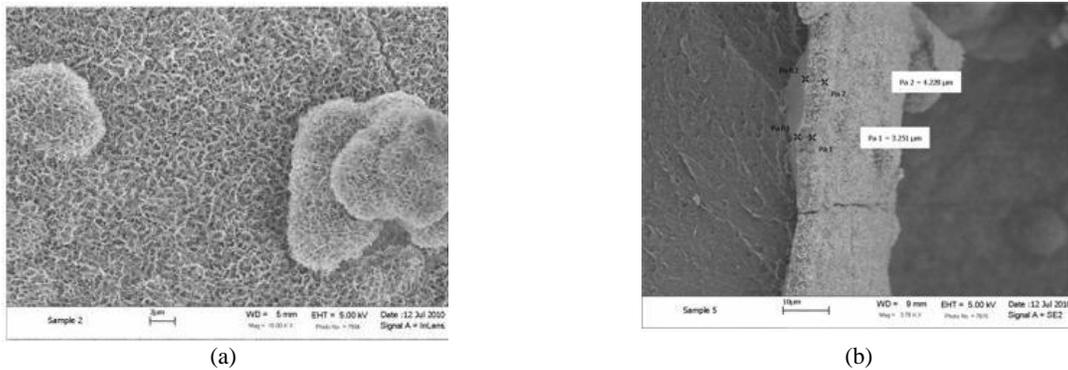
Figure 9. a) The mineral coating and clusters have the same surface morphology (10000x zoom). b) The mineral coating is ~0.003-0.004 mm thick (3.78k x zoom).

5. CLOSURE AND FUTURE WORK

To alleviate material limitations found in existing AM scaffold fabrication process, the authors present an indirect scaffold fabrication process. Following the fabrication of scaffold patterns via FDM, the patterns undergo a surface treatment and mineralization post-process. The patterns, now coated in biocompatible ceramic minerals, will then be heat treated to remove the thermoplastic pattern and to sinter the coating. This approach removes the geometric limitations imposed by existing indirect fabrication approaches that are centered in investment casting with viscous slurries. Furthermore, this approach will result in the fabrication of unique hollow-tube scaffold geometries, increasing scaffold porosity and providing sites suited for vascularization.

In this paper, the authors present the results of their experiments with scaffold pattern fabrication and ceramic mineralization. Two scaffold pattern materials were tested: investment casting wax and ABS. While investment casting wax is better suited for the sintering post-process, it was found not to be suitable for mineralization despite a sodium hydroxide surface treatment. Following a surface treatment with oxygen plasma, the ABS scaffold pattern was observed to have a mineral coating on all surfaces.

With the scaffold patterns fabricated and successfully mineralized, the authors begin exploration of the heat pyrolysis and sintering post-process. It is expected that a sintering temperature of ~1300 °C is needed to burn out the ABS and to sinter the ceramic crystals. In order to ensure that the ceramic coating will survive the proposed heat treatment, the authors must continue to optimize the fabrication process to increase the thickness of the coating (via a longer mineralization procedure) and to remove the cracks observed in the coating (via annealing).

6. REFERENCES

1. Thomas Boland, T.X., Brook Damon, Xiaofeng Cui,, *Application of inkjet printing to tissue engineering.* Biotechnology Journal, 2006. **1**(9): p. 910-917.
2. Tsuruga, E., et al., *Pore Size of Porous Hydroxyapatite as the Cell-Substratum Controls BMP-Induced Osteogenesis.* J Biochem, 1997. **121**(2): p. 317-324.
3. Ayad, S., *The extracellular matrix factsbook.* 2nd ed. Factsbook series. 1998, San Diego: Academic Press. x, 301 p.
4. Lukashev, M.E. and Z. Werb, *ECM signalling: orchestrating cell behaviour and misbehaviour.* Trends in Cell Biology, 1998. **8**(11): p. 437-441.
5. Grinnell, F., *Fibronectin and wound healing.* J Cell Biochem, 1984. **26**(2): p. 107-16.
6. Mecham, R.P., J.G. Madaras, and R.M. Senior, *Extracellular matrix-specific induction of elastogenic differentiation and maintenance of phenotypic stability in bovine ligament fibroblasts.* J Cell Biol, 1984. **98**(5): p. 1804-12.
7. Hutmacher, D.W., *Scaffolds in tissue engineering bone and cartilage.* Biomaterials, 2000. **21**(24): p. 2529-2543.

8. Mikos, A.G., et al., *Prevascularization of porous biodegradable polymers.* Biotechnology and Bioengineering, 1993. **42**(6): p. 716-723.

9. JEFFREY O. HOLLINGER and JOHN P. SCHMITZ, *Macrophysiologic Roles of a Delivery System for Vulnerary Factors Needed for Bone Regeneration.* Annals of the New York Academy of Sciences, 1997. **831**(Bioartificial Organs: Science, Medicine, and Technology): p. 427-437.

10. Zeltinger, J., et al., *Effect of Pore Size and Void Fraction on Cellular Adhesion, Proliferation, and Matrix Deposition.* Tissue Engineering, 2001. **7**(5): p. 557-572.

11. van Tienen, T.G., et al., *Tissue ingrowth and degradation of two biodegradable porous polymers with different porosities and pore sizes.* Biomaterials, 2002. **23**(8): p. 1731-1738.

12. Karande, T.S., J.L. Ong, and C.M. Agrawal, *Diffusion in Musculoskeletal Tissue Engineering Scaffolds: Design Issues Related to Porosity, Permeability, Architecture, and Nutrient Mixing.* Annals of Biomedical Engineering, 2004. **32**(12): p. 1728-1743.

13. Lieberman, J., A. Daluiski, and T. Einhorn, *The role of growth factors in the repair of bone: biology and clinical applications.* The journal of bone and joint surgery, 2002. **84**(6): p. 1032.

14. Babensee, J., L. McIntire, and A. Mikos, *Growth factor delivery for tissue engineering.* Pharmaceutical research, 2000. **17**(5): p. 497-504.

15. Canalis, E., T. McCarthy, and M. Centrella, *Growth factors and the regulation of bone remodeling.* bone, 1987. **13**: p. 14.

16. Mikos, A., et al., *Preparation and characterization of poly (L-lactic acid) foams.* Polymer, 1994. **35**(5): p. 1068-1077.

17. Mooney, D., et al., *Novel approach to fabricate porous sponges of poly (-lactic-co-glycolic acid) without the use of organic solvents.* Biomaterials, 1996. **17**(14): p. 1417-1422.

18. Harris, L., B. Kim, and D. Mooney, *Open pore biodegradable matrices formed with gas foaming.* Journal of Biomedical Materials Research Part A, 1998. **42**(3): p. 396-402.

19. Wei, G. and P.X. Ma, *Structure and properties of nano-hydroxyapatite/polymer composite scaffolds for bone tissue engineering.* Biomaterials, 2004. **25**(19): p. 4749-4757.

20. Oliveira, J.M., et al., *Novel hydroxyapatite/chitosan bilayered scaffold for osteochondral tissue-engineering applications: Scaffold design and its performance when seeded with goat bone marrow stromal cells.* Biomaterials, 2006. **27**(36): p. 6123-6137.

21. Lloyd, D.R., K.E. Kinzer, and H.S. Tseng, *Microporous membrane formation via thermally induced phase separation. I. Solid-liquid phase separation.* Journal of Membrane Science, 1990. **52**(3): p. 239-261.

22. Zein, I., et al., *Fused deposition modeling of novel scaffold architectures for tissue engineering applications.* Biomaterials, 2002. **23**(4): p. 1169-1185.

23. Grida, I. and J.R.G. Evans, *Extrusion freeforming of ceramics through fine nozzles.* Journal of the European Ceramic Society, 2003. **23**(5): p. 629-635.

24. Xiong, Z., et al., *Fabrication of porous scaffolds for bone tissue engineering via low-temperature deposition.* Scripta Materialia, 2002. **46**(11): p. 771-776.

25. Yan, Y., et al., *Layered manufacturing of tissue engineering scaffolds via multi-nozzle deposition.* Materials Letters, 2003. **57**(18): p. 2623-2628.

26. Liu, L., et al., *Porous morphology, porosity, mechanical properties of poly(alpha-hydroxy acid)-tricalcium phosphate composite scaffolds fabricated by low-temperature deposition.* Journal of Biomedical Materials Research Part A, 2007. **82A**(3): p. 618-629.

27. Vozzi, G., et al., *Fabrication of PLGA scaffolds using soft lithography and microsyringe deposition.* Biomaterials, 2003. **24**(14): p. 2533-2540.

28. Landers, R., et al., *Fabrication of soft tissue engineering scaffolds by means of rapid prototyping techniques.* Journal of Materials Science, 2002. **37**(15): p. 3107-3116.

29. Andreas Pfister, R.L., Andres Laib, Ute Hübner, Rainer Schmelzeisen, Rolf Mülhaupt,, *Biofunctional rapid prototyping for tissue-engineering applications: 3D bioplotting versus 3D printing.* Journal of Polymer Science Part A: Polymer Chemistry, 2004. **42**(3): p. 624-638.

30. Miranda, P., et al., *Sintering and robocasting of [beta]-tricalcium phosphate scaffolds for orthopaedic applications.* Acta Biomaterialia, 2006. **2**(4): p. 457-466.

31. Smay, J.E., J. Cesarano, and J.A. Lewis, *Colloidal Inks for Directed Assembly of 3-D Periodic Structures.* Langmuir, 2002. **18**(14): p. 5429-5437.

32. Dellinger, J.G., C. Joseph, III, and D.J. Russell (2007) *Robotic deposition of model hydroxyapatite scaffolds with multiple architectures and multiscale porosity for bone tissue engineering*. Journal of Biomedical Materials Research Part A, 383-394 DOI: 10.1002/jbm.a.31072.

33. Lewis, J.A., *Colloidal Processing of Ceramics.* Journal of the American Ceramic Society, 2000. **83**(10): p. 2341-2359.

34. Mironov, V., G. Prestwich, and G. Forgacs, *Bioprinting living structures.* Journal of Materials Chemistry, 2007. **17**(20): p. 2054-2060.

35. Seitz, H., et al., *Three-dimensional printing of porous ceramic scaffolds for bone tissue engineering.* Journal of Biomedical Materials Research Part B: Applied Biomaterials, 2005. **74B**(2): p. 782-788.

36. Taboas, J., et al., *Indirect solid free form fabrication of local and global porous, biomimetic and composite 3D polymer-ceramic scaffolds.* Biomaterials, 2003. **24**(1): p. 181-194.

37. Hetzer, R.S.M.L.A.H.D.M.S.H.E.P.H.H.T.L.R., *Application of Stereolithography for Scaffold Fabrication for Tissue Engineered Heart Valves.* ASAIO, 2002.

38. Arcaute, K., B. Mann, and R. Wicker, *Stereolithography of Three-Dimensional Bioactive Poly(Ethylene Glycol) Constructs with Encapsulated Cells.* Annals of Biomedical Engineering, 2006. **34**(9): p. 1429-1441.

39. Lee, M., J. Dunn, and B. Wu, *Scaffold fabrication by indirect three-dimensional printing.* Biomaterials, 2005. **26**(20): p. 4281-4289.

40. Chu, T., et al., *Hydroxyapatite implants with designed internal architecture.* Journal of Materials Science: Materials in Medicine, 2001. **12**(6): p. 471-478.

41. Yeong, W., et al., *Indirect fabrication of collagen scaffold based on inkjet printing technique.* Rapid Prototyping Journal, 2006. **12**(4): p. 229-237.

42. Detsch, R., et al., *3D-Cultivation of bone marrow stromal cells on hydroxyapatite scaffolds fabricated by dispense-plotting and negative mould technique.* Journal of Materials Science: Materials in Medicine, 2008. **19**(4): p. 1491-1496.

43. Sachlos, E., et al., *Novel collagen scaffolds with predefined internal morphology made by solid freeform fabrication.* Biomaterials, 2003. **24**(8): p. 1487-1497.

44. Müller, L. and F.A. Müller, *Preparation of SBF with different content and its influence on the composition of biomimetic apatites.* Acta Biomaterialia, 2006. **2**(2): p. 181-189.

45. Kokubo, T. and H. Takadama, *How useful is SBF in predicting in vivo bone bioactivity?* Biomaterials, 2006. **27**(15): p. 2907-2915.

46. Kretlow, J. and A. Mikos, *Review: mineralization of synthetic polymer scaffolds for bone tissue engineering.* Tissue Engineering, 2007. **13**(5): p. 927-938.

47. Zhang, R. and P. Ma, *Biomimetic polymer/apatite composite scaffolds for mineralized tissue engineering.* Macromolecular Bioscience, 2004. **4**(2): p. 100-111.

48. Li, J., et al., *Transfer of apatite coating from porogens to scaffolds: Uniform apatite coating within porous poly(DL-lactic-co-glycolic acid) scaffold in vitro.* Journal of Biomedical Materials Research Part A, 2007. **80A**(1): p. 226-233.

49. Yang, F., J. Wolke, and J. Jansen, *Biomimetic calcium phosphate coating on electrospun poly (-caprolactone) scaffolds for bone tissue engineering.* Chemical Engineering Journal, 2008. **137**(1): p. 154-161.

50. Venugopal, J., et al., *Electrospun-modified nanofibrous scaffolds for the mineralization of osteoblast cells.* Journal of Biomedical Materials Research Part A, 2008. **85**(2): p. 408-417.